LETTER

doi:10.1038/nature14404

Melanoma-intrinsic β-catenin signalling prevents anti-tumour immunity

Stefani Spranger[1], Riyue Bao[2] & Thomas F. Gajewski[1,3]

Melanoma treatment is being revolutionized by the development of effective immunotherapeutic approaches[1,2]. These strategies include blockade of immune-inhibitory receptors on activated T cells; for example, using monoclonal antibodies against CTLA-4, PD-1, and PD-L1 (refs 3–5). However, only a subset of patients responds to these treatments, and data suggest that therapeutic benefit is preferentially achieved in patients with a pre-existing T-cell response against their tumour, as evidenced by a baseline CD8$^+$ T-cell infiltration within the tumour microenvironment[6,7]. Understanding the molecular mechanisms that underlie the presence or absence of a spontaneous anti-tumour T-cell response in subsets of cases, therefore, should enable the development of therapeutic solutions for patients lacking a T-cell infiltrate. Here we identify a melanoma-cell-intrinsic oncogenic pathway that contributes to a lack of T-cell infiltration in melanoma. Molecular analysis of human metastatic melanoma samples revealed a correlation between activation of the WNT/β-catenin signalling pathway and absence of a T-cell gene expression signature. Using autochthonous mouse melanoma models[8,9] we identified the mechanism by which tumour-intrinsic active β-catenin signalling results in T-cell exclusion and resistance to anti-PD-L1/anti-CTLA-4 monoclonal antibody therapy. Specific oncogenic signals, therefore, can mediate cancer immune evasion and resistance to immunotherapies, pointing to new candidate targets for immune potentiation.

To identify oncogenic pathways inversely associated with T-cell infiltration, we categorized 266 metastatic human cutaneous melanoma samples into those with low (non-T-cell-inflamed) and high (T-cell-inflamed) expression of T-cell signature genes[6,10] (Fig. 1a). Comparative gene expression profiling revealed 1,755 genes that were preferentially expressed in the non-inflamed patient cohort ($q < 0.01$) (Supplementary Table 1). Pathway analysis, comparing 91 non-T-cell-inflamed to 106 T-cell-inflamed patients, indicated active β-catenin signalling (*APC2*, *SOX2*, *SOX11* and *WNT7B*; $P = 0.00116$) as well as dermatan-sulfate biosynthesis (*HS6ST2* and *NDST3*; $P = 0.00196$) in the non-T-cell-inflamed cohort. Previous reports suggested that active β-catenin signalling in melanoma was associated with more aggressive disease[9]. To determine if activation of the β-catenin pathway might be modified by specific mutations, we analysed exome-sequencing data for all 197 patients. Indeed, seven tumour samples (7.7%) with the non-T-cell-inflamed phenotype showed gain-of-function mutations in β-catenin (*CTNNB1*), versus one case in the T-cell-infiltrated cohort. Additionally, loss-of-function mutations in negative regulators of the pathway (*APC*, *AXIN1*, *TCF1*) were identified in ten non-T-cell-inflamed tumours (11%) (Supplementary Table 3). To identify the total percentage of tumours with an active β-catenin pathway, we assessed expression of six well-characterized β-catenin target genes[11]. Forty-eight per cent (44 patients) in the non-T-cell-inflamed subset showed expression of at least five of the six β-catenin target genes versus 3.8% (4 patients) of the T-cell-inflamed tumours (Fig. 1b). While several cases were associated with defined mutations (*CTNNB1*, 14%; *APC*, *AXIN1* or *TCF1*, 23%) the majority (61%) of the remaining cases showed increased expression of either WNT7B (WNT7B, 29.5%; 13 patients), FZD3 (FZD3, 20.5%; 9 patients), or β-catenin itself (11%; 5 patients; Supplementary Table 3). In sum, an increased *CTNNB1* score was predictive for the lack of T cells, with an odds ratio of 4.9 (Extended Data Fig. 1a). Additional analysis revealed a negative correlation between individual β-catenin target genes and *CD8A* transcripts, which was opposite to the pattern of PD-L1 expression (Fig. 1c and Supplementary Table 2)[12]. Immunohistochemical analysis of an independent sample cohort also revealed an inverse association between stabilized β-catenin and CD8$^+$ T cells (Fig. 1d and Extended Data Fig. 1b).

We investigated directly whether active β-catenin signalling within tumour cells could adversely affect anti-tumour T-cell responses using inducible autochthonous mouse models (genetically engineered mice (GEM)) driven by conditional active Braf with or without conditional PTEN deletion and expression of active β-catenin. These GEMs developed tumours with similar latency, as reported previously (Fig. 1e and Extended Data Fig. 2a–c)[8,9]. We focused on *Braf*^{V600E}/*Pten*$^{-/-}$ and *Braf*^{V600E}/*Pten*$^{-/-}$/*CAT-STA* mice due to the similar rate of onset of tumour development in these strains (Extended Data Fig. 2b, c). Using gene array analysis and histological examination we confirmed that the developing tumours were indeed melanomas (Extended Data Fig. 2d, e)[8,9], albeit with less pigmentation in *Braf*^{V600E}/*Pten*$^{-/-}$ tumours (Extended Data Figs 2e, f and 3a, b)[9]. Analysis of immune infiltrates revealed that *Braf*^{V600E}/*Pten*$^{-/-}$ tumours indeed contained CD3$^+$ T cells. However, tumours with active β-catenin showed almost a complete absence of T cells (Fig. 1f). Fluorescent immunohistology confirmed the absence of intratumoural CD3$^+$ T cells in *Braf*^{V600E}/*Pten*$^{-/-}$/*CAT-STA* tumours (Fig. 1g and Extended Data Fig. 3a–c) with only rare T cells observed in the epidermis. These results indicate that tumour-intrinsic β-catenin activation dominantly excludes T-cell infiltration into the melanoma tumour microenvironment.

The T-cell infiltrate in *Braf*^{V600E}/*Pten*$^{-/-}$ tumours consisted of both CD4$^+$ and CD8$^+$ T cells, with the majority of them expressing the αβ-T-cell antigen receptor (TCR) (Extended Data Fig. 4a, b). The majority were CD44^{hi}/CD62L^{lo}/CD45RA^{lo}, suggesting an activated phenotype (Extended Data Fig. 4c), and 6% FoxP3$^+$ regulatory T cells were detected (Extended Data Fig. 4d). Additionally, CD8$^+$ T cells from *Braf*^{V600E}/*Pten*$^{-/-}$ tumours showed expression of PD-1 and Lag3 (Extended Data Fig. 4e, f), markers of T-cell dysfunction in the tumour context[13]. Consistent with this phenotype, sorted CD3$^+$ T cells from *Braf*^{V600E}/*Pten*$^{-/-}$ tumours showed defective interleukin (IL)-2 production but were capable of producing interferon (IFN)-γ (Extended Data Fig. 4g, h). Comparable studies on the few T cells from *Braf*^{V600E}/*Pten*$^{-/-}$/*CAT-STA* tumours showed predominantly a naive phenotype (Extended Data Fig. 4a–e). Correspondingly, increased PD-L1 expression in *Braf*^{V600E}/*Pten*$^{-/-}$ tumours was observed, consistent with previous work linking PD-L1 expression with the presence of CD8$^+$ T cells (Extended Data Fig. 4i, j)[12]. We did not detect significant differences in CD11b$^+$Gr1$^+$ myeloid-derived suppressor cells

[1]Department of Pathology, The University of Chicago, Chicago, Illinois 60637, USA. [2]Center for Research Informatics, The University of Chicago, Chicago, Illinois 60637, USA. [3]Department of Medicine, The University of Chicago, Chicago, Illinois 60637, USA.

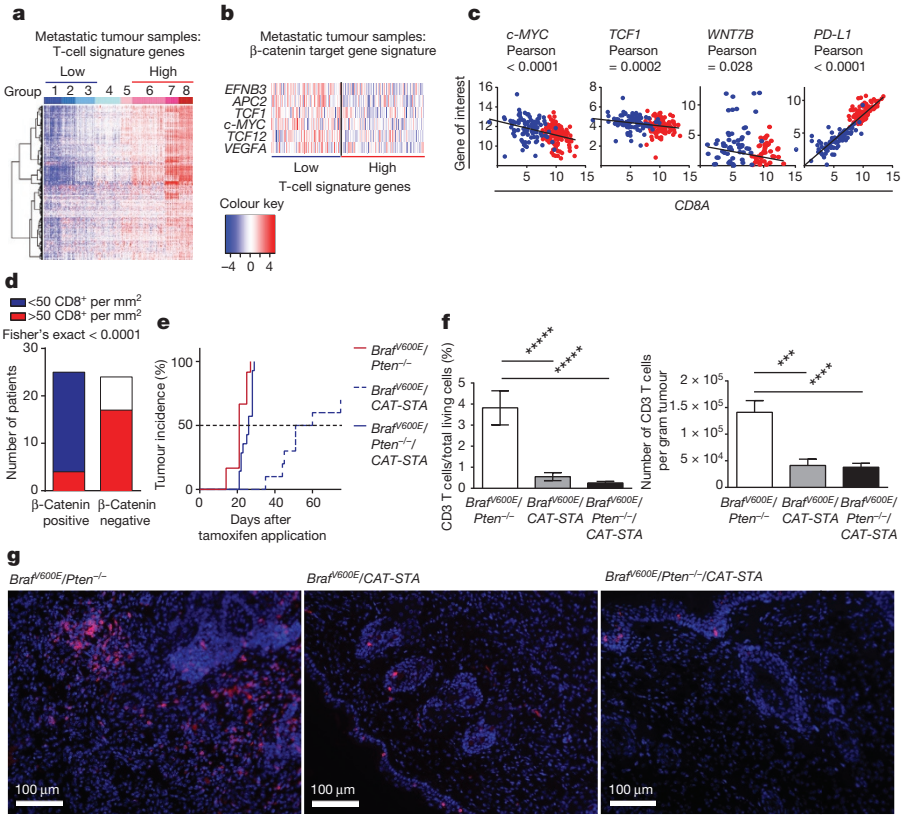

Figure 1 | Melanoma-intrinsic β-catenin pathway activation correlates with T-cell exclusion. a, **b**, Heat maps of 266 metastatic melanomas clustered in low versus high T-cell signature gene groups (**a**), and β-catenin target genes within the T-cell-signature high and low cohorts (**b**). **c**, Pearson correlation of *CD8A* expression with c-MYC, TCF1 and WNT7B (red indicates T-cell-signature high, blue indicates T-cell-signature low). **d**, Correlation between β-catenin and CD8 in melanoma biopsies. Fisher's exact test with $n = 49$. **e**, Tumour incidence rates of GEMs (median time to tumour event): $Braf^{V600E}/Pten^{-/-}$: 100%, 21 days ($n = 14$); $Braf^{V600E}/CAT\text{-}STA$: 85%, 55.5 days ($n = 8$); $Braf^{V600E}/Pten^{-/-}/CAT\text{-}STA$: 100%, 26 days ($n = 14$). **f**, $CD3^+$ T cells depicted as percentage living cells and absolute numbers per gram tumour. $n = 20$, mean ± standard error of the mean (s.e.m.), Mann–Whitney *U* test. **g**, Representative example out of five for fluorescent immunohistochemistry staining against $CD3^+$ T cells. Scale bars, 100 µm. See Extended Data Fig. 3 for overview. $^{***}P \leq 0.001$, $^{****}P \leq 0.0001$, $^{*****}P \leq 0.00001$.

($Braf^{V600E}/Pten^{-/-}$, 1,047 ± 418, to $Braf^{V600E}/Pten^{-/-}/CAT\text{-}STA$, 739 ± 185 cells per gram tumour; $P = 0.7429$) (Extended Data Fig. 4k)[14].

Although the models used in this study recapitulate defined carcinogenic processes, one drawback is the potentially low number of generated neo-antigens, which may lead to reduced immunogenicity[15]. To circumvent this we crossed both GEMs to a mouse strain allowing Cre-dependent expressing of the model antigen SIYRYYGL (SIY)[16]. We investigated whether lack of T-cell infiltration into the $Braf^{V600E}/Pten^{-/-}/CAT\text{-}STA$ tumours was secondary to a lack of initial T-cell priming by adoptive transfer of carboxyfluorescein succinimidyl ester (CFSE)-labelled SIY-specific TCR-transgenic 2C T cells. While SIY-negative mice failed to accumulate 2C T cells within the tumour-draining lymph nodes (TdLNs) or the tumour site, SIY-positive mice had detectable 2C T cells in the TdLNs in both GEMs. However, no proliferation of 2C T cells was identified within the TdLNs in the $Braf^{V600E}/Pten^{-/-}/CAT\text{-}STA/SIY^+$ model, whereas activation of T cells within the TdLNs of $Braf^{V600E}/Pten^{-/-}$ mice was brisk (Fig. 2a, b). Accordingly, the presence of proliferated 2C T cells was observed at the tumour site exclusively in $Braf^{V600E}/Pten^{-/-}$ mice (Fig. 2a, b). These data indicate that tumour-intrinsic β-catenin signalling prevents the early steps of T-cell priming against tumour-associated antigens.

The absence of early T-cell priming in $Braf^{V600E}/Pten^{-/-}/CAT\text{-}STA$ tumour-bearing mice suggested a defect in the antigen-presenting-cell compartment. Work using transplantable tumour models has indicated that Batf3-lineage dendritic cells are crucial for cross-presentation of tumour antigens to $CD8^+$ T cells[17–19]. Dendritic cell subsets ($CD45^+MHCII^+CD11c^+$) were analysed phenotypically within the tumour microenvironment with minimal differences observed in the number of conventional dendritic cells ($B220^-$), plasmacytoid dendritic cells ($B220^+$), monocytes ($B220^-Ly6C^+$), or Langerhans dendritic cells ($B220^-CD207^+$). Strikingly, the $CD8\alpha^+$ and $CD103^+$ dendritic cell populations were nearly completely absent from $Braf^{V600E}/Pten^{-/-}/CAT\text{-}STA$ tumours (Fig. 2c–e). $CD103^+$ dendritic cells were also reduced in the TdLNs, while being preserved in the spleen (Fig. 2d, e; data not shown). Sorted tumour-infiltrating $CD45^+CD11c^+$ dendritic cells from $Braf^{V600E}/Pten^{-/-}/CAT\text{-}STA$ tumours also showed reduced expression of the $CD103^+$ dendritic cell transcripts *Batf3*, *Irf8* and *Itgae* (Extended Data Fig. 5a, b), and dendritic cells showed reduced expression of the key innate cytokine IFN-β (Extended Data Fig. 5a). Together, these results suggest that the failed T-cell priming against tumour-associated antigen in $Braf^{V600E}/Pten^{-/-}/CAT\text{-}STA$ tumours is secondary to defective recruitment and activation of Batf3-lineage dendritic cells.

To determine whether T-cell infiltration into $Braf^{V600E}/Pten^{-/-}$ tumours was dependent on $CD103^+$ dendritic cells, $Batf3^{-/-}$ bone marrow chimaeras were generated. Indeed, tumours from $Braf^{V600E}/Pten^{-/-}/Batf3^{-/-}$ bone marrow chimaeras failed to develop T-cell infiltration (Fig. 2f). To assess whether poor dendritic cell recruitment was indeed the major functional barrier, we generated Flt3 ligand-derived bone-marrow dendritic cells activated with polyinosinic:polycytidylic acid (poly(I:C))[20] for intra-tumoural injection, which were found to restore T-cell infiltration in $Braf^{V600E}/Pten^{-/-}/CAT\text{-}STA$ tumours (Fig. 2h) and led to a modest reduction in tumour weight

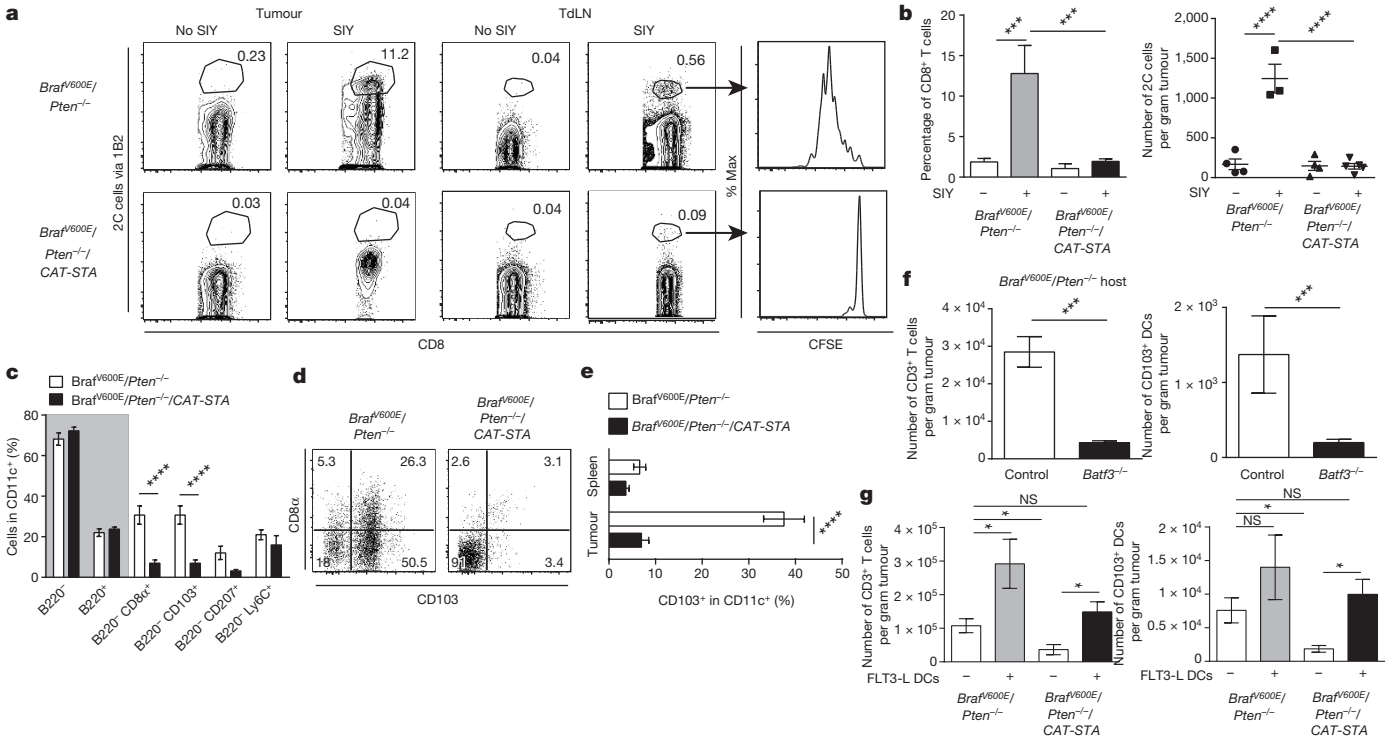

Figure 2 | *Braf*^{V600E}/*Pten*$^{-/-}$/*CAT-STA* mice show impaired priming of anti-tumour T cells and reduced numbers of CD103$^+$ dermal dendritic cells. **a**, Abundance and proliferation of TCR-transgenic 2C T cells. Depicted are representative examples pre-gated on live, CD45$^+$CD3$^+$CD8$^+$ cells. **b**, Statistical analysis of **a** ($n = 8$). **c**, Percentages of dendritic cell subsets within *Braf*^{V600E}/*Pten*$^{-/-}$ and *Braf*^{V600E}/*Pten*$^{-/-}$/*CAT-STA* tumours ($n = 8$). **d**, Representative example of CD103/CD8α staining (gated CD45$^+$MHCII^{hi}CD11c$^+$). **e**, Quantification of CD103$^+$ dendritic cells ($n = 12$). **f**, Amount of CD3$^+$ T cell and CD103$^+$ dendritic cell (DC) infiltration in *Braf*^{V600E}/*Pten*$^{-/-}$ tumours reconstituted with control or *Batf3*$^{-/-}$ bone marrow ($n = 4$ and $n = 11$, respectively). **g**, Intra-tumoural injection of Flt3 ligand-derived dendritic cells into *Braf*^{V600E}/*Pten*$^{-/-}$/*CAT-STA* tumours ($n = 6$ control mice and 8 mice, PBS control). All data are mean ± s.e.m., Mann–Whitney *U* test. $*P \leq 0.05$, $***P \leq 0.001$, $****P \leq 0.0001$; NS, not significant.

(Extended Data Fig. 5c). Using dendritic cells generated from actin–green fluorescent protein (GFP) transgenic mice, injected dendritic cells were retained within the tumour microenvironment during this experimental timeframe (Extended Data Fig. 5d). Together, these results suggest that the major immunological defect in the context of melanomas expressing tumour-intrinsic β-catenin signalling is defective recruitment of CD103$^+$ dendritic cells.

To pursue mechanisms explaining failed CD103$^+$ dermal dendritic cell recruitment, gene expression profiling was performed from tumours of the two genotypes, focusing on chemokines (Supplementary Table 4). Five chemokines were differentially expressed, with four of these (*CCL3*, *CXCL1*, *CXCL2* and *CCL4*) being expressed at lower levels in *Braf*^{V600E}/*Pten*$^{-/-}$/*CAT-STA* tumours (Fig. 3a, b and Supplementary Table 4). For evaluation of tumour-cell-intrinsic chemokine production *in vivo*, we crossed *Braf*^{V600E}/*Pten*$^{-/-}$ mice to yellow fluorescent protein (YFP)-reporter mice, which allowed identification of transformed YFP$^+$ cells. *Ccl4* transcripts were detected exclusively in the YPF$^+$ cell population from *Braf*^{V600E}/*Pten*$^{-/-}$ mice, while control sorted YFP$^+$ cells from *Braf*^{WT}/*Pten*$^{-/-}$ mice or YFP$^-$ cells showed no detectable *Ccl4* (Fig. 3c). A similar expression pattern was observed for *CXCL1*, whereas *CCL3* and *CXCL2* were expressed by normal melanocytes and stromal cells, respectively (Fig. 3c). CD45$^+$CD3$^+$ and CD45$^+$CD3$^-$ cells sorted as controls, showing the expected patterns of *Ifng* and *Ifnb* expression (Extended Data Fig. 6c, d). Expression analysis of the corresponding chemokine receptor, *Ccr5*, revealed a lack of CCR5 expression by the dendritic cells isolated from *Braf*^{V600E}/*Pten*$^{-/-}$/*CAT-STA* tumours (Fig. 3d). CCR5 has previously been linked with the migratory capacity of CD8α$^+$ dendritic cells[21]. To confirm this observation, we generated tumour cell lines from both GEMs and found increased production of CCL4 by BP (*Braf*^{V600E}/*Pten*$^{-/-}$-derived) tumour cells compared to BPC (*Braf*^{V600E}/*Pten*$^{-/-}$/*CAT-STA*-derived) tumour cells (Extended Data Fig. 6a, b). To strengthen a functional role for CCL4, we used an *in vitro* migration assay in response to recombinant murine CCL4 as well as tumour cell line supernatants (Fig. 3e). Indeed, skin-derived CD11c$^+$CD103$^+$ dendritic cells and lymph-node-derived dendritic cells (CD11c$^+$CD8α$^+$) migrated in response to CCL4 and BP supernatants but not to BPC supernatants. Together, these results indicate that failed recruitment of CD103$^+$ dendritic cells into the tumour microenvironment of *Braf*^{V600E}/*Pten*$^{-/-}$/*CAT-STA* tumours was, at least in part, due to defective production of the chemokine CCL4.

We then pursued a mechanism by which β-catenin activation might prevent *Ccl4* gene expression, since CCL4 has also been associated with a T-cell infiltrate in human melanoma tumours[6,22]. Previous reports had suggested that Wnt/β-catenin signalling induces expression of the transcriptional repressor ATF3 (ref. 23), and that ATF3 suppresses *Ccl4* (ref. 24). Indeed, *Atf3* was expressed at higher levels in primary tumours as well as in BPC tumour cell lines from *Braf*^{V600E}/*Pten*$^{-/-}$/*CAT-STA* mice (Fig. 3f). A chromatin immunoprecipitation (ChIP) assay revealed binding of ATF3 to the *Ccl4* promoter region in *Braf*^{V600E}/*Pten*$^{-/-}$/*CAT-STA* cells while no binding was observed for *Ccl2*, a chemokine lacking an ATF3-binding site (Fig. 3g). Short interfering RNA (siRNA)-mediated knockdown of *Atf3* or *Ctnnb1* in BPC tumour cells restored CCL4 production (Fig. 3h). To examine this relationship in human melanoma, we analysed two melanoma cell lines, mel537 and mel888, which show low or high β-catenin expression, respectively (Extended Data Fig. 7a, c). Consistent with the murine cell lines, increased *ATF3* and decreased CCL4 production were observed in the β-catenin-positive mel888 cells (Extended Data Fig. 7b, e), and increased binding of ATF3 to the *CCL4* promoter was also detected (Extended Data Fig. 7d). siRNA-mediated knockdown of ATF3 or

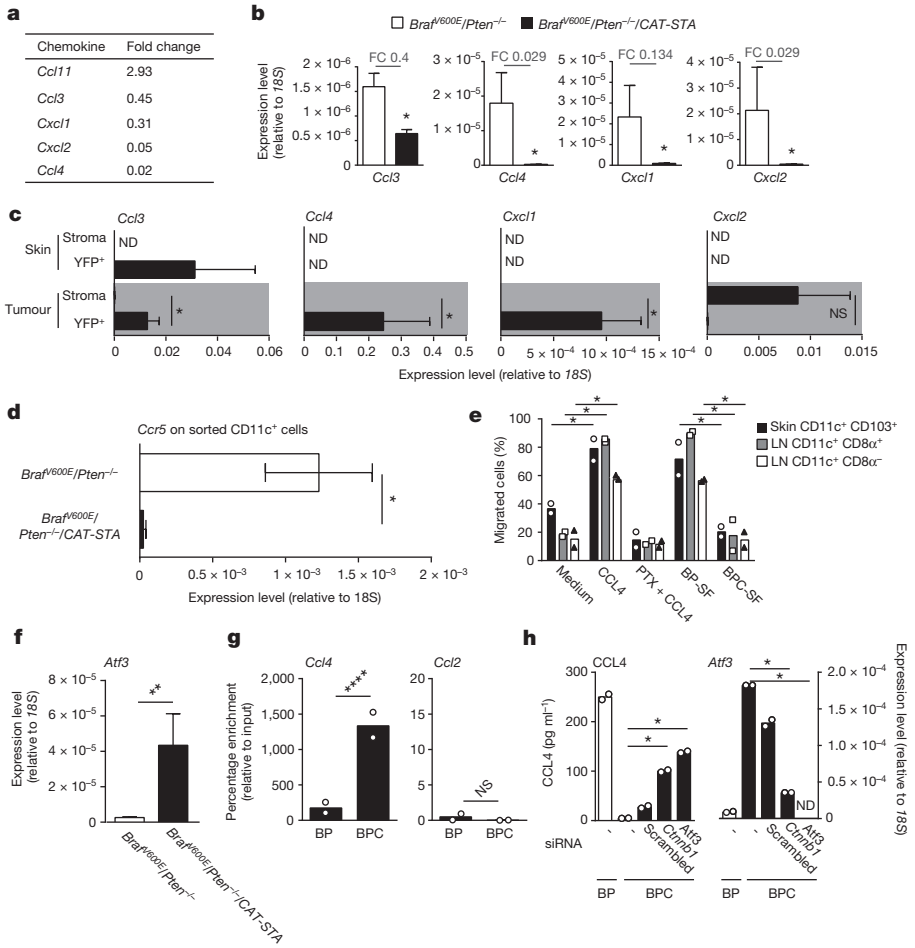

Figure 3 | Active β-catenin signalling within tumour cells suppresses the recruitment of CD103$^+$ dendritic cells. **a**, Chemokine expression in GEM tumours assessed via gene array analysis ($n = 4$). **b**, Confirmatory quantitative polymerase chain reaction with reverse transcription (qRT–PCR) ($n = 8$) with fold change (FC) indicated at the top. **c**, Transcript levels of *Ccl3*, *Ccl4*, *Cxcl1* and *Cxcl2* assessed from YFP$^+$ and CD45$^-$ YFP$^-$ cells from *Braf*^{V600E}/*Pten*$^{-/-}$/YFP$^+$ tumours ($n = 5$), sorted on day 7 after tamoxifen administration. ND, not detected. **d**, Expression level of CCR5 in sorted CD45$^+$CD11c$^+$ dendritic cells ($n = 8$). **e**, Migration assay of dendritic cell subsets towards recombinant mouse CCL4 or conditioned medium (SF) (two independent experiments, duplicates per experiment). **f**, *Atf3* transcripts in tumour tissues ($n = 8$). **g**, ATF3-specific ChIP assay in BP and BPC cell lines (two independent experiments, duplicates per experiment). **h**, Amount of secreted CCL4 in 48-h-conditioned siRNA-treated tumour-cell BP and BPC supernatants, assessed by enzyme-linked immunosorbent assay (ELISA) and *Atf3* expression at the endpoint detected by qRT–PCR (two independent experiments, duplicates per experiment). All data are mean ± s.e.m., Mann–Whitney *U* test. $*P \leq 0.05$, $**P \leq 0.01$, $****P \leq 0.0001$; NS, not significant.

β-catenin in mel888 cells restored CCL4 production (Extended Data Fig. 7e).

We additionally investigated whether decreased presence of BATF3-lineage dendritic cells was associated with active β-catenin signalling in human melanoma metastases. A Pearson correlation analysis for expression of *THBD* (CD141, marker for human BATF3-lineage dendritic cells[25]; $P < 0.0001$), *BATF3* ($P = 0.0336$) and *IRF8* ($P < 0.0001$) revealed a negative association with the *CTNNB1* score (Extended Data Fig. 8 and data not shown). Furthermore, *CCL4* had already been observed to correlate positively with T-cell transcripts (Fig. 1a). We conclude that β-catenin activation within melanoma cells results in decreased *CCL4* gene expression, which is at least partly mediated through ATF3-dependent transcriptional repression (Extended Data Fig. 9).

To explore the therapeutic relevance of the lack of T-cell infiltration, both GEMs were treated with a combination of anti-CTLA-4 and anti-PD-L1 monoclonal antibodies[3,26]. While treatment of *Braf*^{V600E}/*Pten*$^{-/-}$ mice resulted in a significant delay in tumour outgrowth, no therapeutic effect was detected in *Braf*^{V600E}/*Pten*$^{-/-}$/*CAT-STA* mice (Fig. 4a, b). To evaluate whether restoration of intra-tumoural dendritic cells could restore immunotherapy responsiveness, Flt3 ligand-induced bone-marrow dendritic cells were injected intra-tumourally into *Braf*^{V600E}/*Pten*$^{-/-}$/*CAT-STA* tumours. Indeed, introduction of dendritic cells had a partial therapeutic effect, which was improved significantly with anti-CTLA-4 and anti-PD-L1 monoclonal antibodies (Fig. 4c).

We conclude that melanoma-cell-intrinsic activation of an oncogenic pathway can result in exclusion of the host immune response, including the absence of a T-cell infiltrate within the tumour microenvironment. Although 48% of non-T-cell-infiltrated melanomas show active β-catenin signalling, it is conceivable that additional oncogenic signalling pathways might mediate immune exclusion in other cases. The WNT/β-catenin pathway may contribute to immune evasion in other tumour entities beyond melanoma, which would be consistent with previous *in vitro* work[27]. Within T cells, β-catenin appears to inhibit T-cell activation, suggesting that a general immune-potentiating effect may result from therapeutic targeting[28]. The T-cell-inflamed tumour microenvironment phenotype appears to be predictive of clinical response to immune-based therapies[7,10,29]. Immune escape among this subset appears to be a consequence of dominant effects of negative regulatory pathways such as PD-1, arguing that the clinical activity of anti-PD-1 is tipping the balance in favour of an ongoing immune response[12]. By inference, tumour-intrinsic

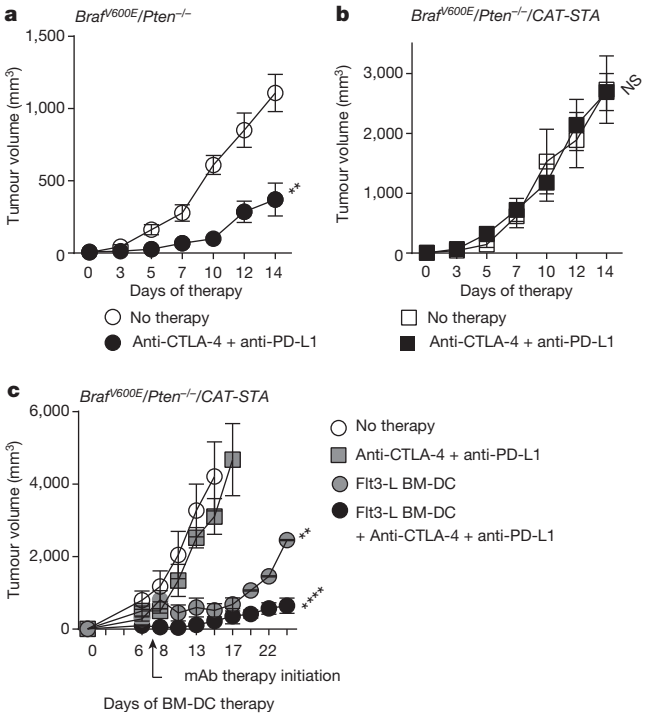

Figure 4 | Reconstitution with Flt3 ligand dendritic cells reverses resistance to immunotherapy. **a**, **b**, Tumour growth in $Braf^{V600E}/Pten^{-/-}$ (**a**) and $Braf^{V600E}/Pten^{-/-}/CAT\text{-}STA$ (**b**) mice untreated or treated with anti-CTLA-4 and anti-PD-L1 therapy ($n = 10$). **c**, Tumour growth of $Braf^{V600E}/Pten^{-/-}/CAT\text{-}STA$ tumour-bearing mice that were untreated, treated with anti-CTLA-4 and anti-PD-L1 therapy, intra-tumoural Flt3 ligand (Flt3-L) dendritic cell injections, or combination therapy ($n = 5$). BM-DC, bone-marrow dendritic cell; mAb, monoclonal antibody. All data are mean ± s.e.m., two-way analysis of variance (ANOVA) test. $^{**}P \leq 0.01$, $^{****}P \leq 0.0001$; NS, not significant.

β-catenin activation may represent one mechanism of primary resistance to these therapies.

Online Content Methods, along with any additional Extended Data display items and Source Data, are available in the online version of the paper; references unique to these sections appear only in the online paper.

Received 15 August 2014; accepted 5 March 2015.
Published online 11 May 2015.

1. Kaufman, H. L. *et al.* The Society for Immunotherapy of Cancer consensus statement on tumour immunotherapy for the treatment of cutaneous melanoma. *Nature Rev. Clin. Oncol.* **10,** 588–598 (2013).
2. Mellman, I., Coukos, G. & Dranoff, G. Cancer immunotherapy comes of age. *Nature* **480,** 480–489 (2011).
3. Wolchok, J. D. *et al.* Nivolumab plus ipilimumab in advanced melanoma. *N. Engl. J. Med.* **369,** 122–133 (2013).
4. Topalian, S. L. *et al.* Survival, durable tumor remission, and long-term safety in patients with advanced melanoma receiving nivolumab. *J. Clin. Oncol.* **32,** 1020–1030 (2014).
5. Hodi, F. S. *et al.* Improved survival with ipilimumab in patients with metastatic melanoma. *N. Engl. J. Med.* **363,** 711–723 (2010).
6. Harlin, H. *et al.* Chemokine expression in melanoma metastases associated with $CD8^+$ T-cell recruitment. *Cancer Res.* **69,** 3077–3085 (2009).
7. Ji, R. R. *et al.* An immune-active tumor microenvironment favors clinical response to ipilimumab. *Cancer Immunol. Immunother.* **61,** 1019–1031 (2012).
8. Dankort, D. *et al.* Braf(V600E) cooperates with Pten loss to induce metastatic melanoma. *Nature Genet.* **41,** 544–552 (2009).
9. Damsky, W. E. *et al.* β-Catenin signaling controls metastasis in Braf-activated Pten-deficient melanomas. *Cancer Cell* **20,** 741–754 (2011).
10. Galon, J. *et al.* Type, density, and location of immune cells within human colorectal tumors predict clinical outcome. *Science* **313,** 1960–1964 (2006).
11. Rimm, D. L., Caca, K., Hu, G., Harrison, F. B. & Fearon, E. R. Frequent nuclear/cytoplasmic localization of β-catenin without exon 3 mutations in malignant melanoma. *Am. J. Pathol.* **154,** 325–329 (1999).
12. Spranger, S. *et al.* Up-regulation of PD-L1, IDO, and T_{regs} in the melanoma tumor microenvironment is driven by $CD8^+$ T cells. *Sci. Transl. Med.* **5,** 200ra116 (2013).
13. Woo, S. R. *et al.* Immune inhibitory molecules LAG-3 and PD-1 synergistically regulate T-cell function to promote tumoral immune escape. *Cancer Res.* **72,** 917–927 (2012).
14. Landsberg, J. *et al.* Melanomas resist T-cell therapy through inflammation-induced reversible dedifferentiation. *Nature* **490,** 412–416 (2012).
15. Matsushita, H. *et al.* Cancer exome analysis reveals a T-cell-dependent mechanism of cancer immunoediting. *Nature* **482,** 400–404 (2012).
16. Cheung, A. F., Dupage, M. J., Dong, H. K., Chen, J. & Jacks, T. Regulated expression of a tumor-associated antigen reveals multiple levels of T-cell tolerance in a mouse model of lung cancer. *Cancer Res.* **68,** 9459–9468 (2008).
17. Fuertes, M. B. *et al.* Host type I IFN signals are required for antitumor $CD8^+$ T cell responses through $CD8\alpha^+$ dendritic cells. *J. Exp. Med.* **208,** 2005–2016 (2011).
18. Hildner, K. *et al.* Batf3 deficiency reveals a critical role for $CD8\alpha^+$ dendritic cells in cytotoxic T cell immunity. *Science* **322,** 1097–1100 (2008).
19. Bedoui, S. *et al.* Cross-presentation of viral and self antigens by skin-derived $CD103^+$ dendritic cells. *Nature Immunol.* **10,** 488–495 (2009).
20. Mollah, S. A. *et al.* Flt3L dependence helps define an uncharacterized subset of murine cutaneous dendritic cells. *J. Invest. Dermatol.* **134,** 1265–1275 (2014).
21. Aliberti, J. *et al.* CCR5 provides a signal for microbial induced production of IL-12 by $CD8\alpha^+$ dendritic cells. *Nature Immunol.* **1,** 83–87 (2000).
22. Peng, W. *et al.* PD-1 blockade enhances T-cell migration to tumors by elevating IFN-γ inducible chemokines. *Cancer Res.* **72,** 5209–5218 (2012).
23. Li, Y. *et al.* N-myc downstream-regulated gene 2, a novel estrogen-targeted gene, is involved in the regulation of Na^+/K^+-ATPase. *J. Biol. Chem.* **286,** 32289–32299 (2011).
24. Khuu, C. H., Barrozo, R. M., Hai, T. & Weinstein, S. L. Activating transcription factor 3 (ATF3) represses the expression of CCL4 in murine macrophages. *Mol. Immunol.* **44,** 1598–1605 (2007).
25. Jongbloed, S. L. *et al.* Human $CD141^+$ $(BDCA\text{-}3)^+$ dendritic cells (DCs) represent a unique myeloid DC subset that cross-presents necrotic cell antigens. *J. Exp. Med.* **207,** 1247–1260 (2010).
26. Spranger, S. *et al.* Mechanism of tumor rejection with doublets of CTLA-4, PD-1/PD-L1, or IDO blockade involves restored IL-2 production and proliferation of $CD8^+$ T cells directly within the tumor microenvironment. *J. Immunother. Cancer* (2014).
27. Yaguchi, T. *et al.* Immune suppression and resistance mediated by constitutive activation of Wnt/β-catenin signaling in human melanoma cells. *J. Immunol.* **189,** 2110–2117 (2012).
28. Driessens, G. *et al.* β-Catenin inhibits T cell activation by selective interference with linker for activation of T cells–phospholipase C-γ1 phosphorylation. *J. Immunol.* **186,** 784–790 (2011).
29. Cipponi, A., Wieers, G., van Baren, N. & Coulie, P. G. Tumor-infiltrating lymphocytes: apparently good for melanoma patients. But why? *Cancer Immunol. Immunother.* **60,** 1153–1160 (2011).

Supplementary Information is available in the online version of the paper.

Acknowledgements The authors would like to thank A. Sailer and J. Turner for their assistance on mouse tissue immunofluorescent staining, M. Leung and Y. Zha for technical support, and the Special Services Animal Resources Center for assistance with mouse husbandry. We also acknowledge the Fitch Monoclonal Antibody Facility, the Human Tissue Research Core and the Integrated Microscopy core of The University of Chicago Comprehensive Cancer Center. We would like to thank A. O. Emmanuel and F. Gounari for assistance with the ChIP assay as well as for conditional β-catenin knock-in mice; C. Slingluff, D. Deacon, J. Schaefer, G. Erdag and the University of Virginia Biorepository and Tissue Research Facility for melanoma biopsy specimens, and P. Savage for critical comments. Funding for this study was provided by a Team Science Award from the Melanoma Research Alliance and a Translational Research Grant from the Cancer Research Institute. S.S. was supported by the German Research Foundation and is currently a fellow of the Cancer Research Institute.

Author Contributions S.S. contributed to the overall project design, planned and performed experiments, and performed data analysis. R.B. performed analysis of the TCGA data set. T.F.G. designed the overall project. S.S. and T.F.G. wrote the manuscript.

Author Information Gene array data have been deposited in the Gene Expression Omnibus under accession number GSE63543. Reprints and permissions information is available at www.nature.com/reprints. The authors declare no competing financial interests. Readers are welcome to comment on the online version of the paper. Correspondence and requests for materials should be addressed to T.F.G. (tgajewsk@medicine.bsd.uchicago.edu).

METHODS

Analysis of TCGA data set. Level 4 gene expression data and level 2 somatic mutation data were downloaded for skin cutaneous melanoma (SKCM) from TCGA, which were processed by Broad Institute's TCGA workgroup (release date 10 October 2013). The RNA-seq level 4 gene expression data contain upper-quartile-normalized and $\log_2$-transformed RNA-seq by expectation maximization (RSEM) values summarized at gene level[30]. The whole-exome sequencing (WXS) level 2 mutation data contains somatic mutation calls for each subject. A total of 266 metastatic SKCM samples were analysed. For clustering of cold and hot tumours, genes expressed in less than 80% of the samples were removed. A total of 15,974 genes were kept for further analysis. Unsupervised hierarchical clustering of the genes was performed in primary tumours and metastasis samples separately using *K*-mean equal to 12 and Euclidean distance metrics. Clusters containing the 13 known T-cell-signature transcripts (*CD8A*, *CCL2*, *CCL3*, *CCL4*, *CXCL9*, *CXCL10*, *ICOS*, *GZMK*, *IRF1*, *HLA-DMA*, *HLA-DMB*, *HLA-DOA*, *HLA-DOB*) were selected for resampling-based hierarchical clustering of the samples using ConsensusClusterPlus v.1.16.0 (ref. 31). This procedure was performed with 2,000 random selections of 80% of the samples and Euclidean distance metrics. Genes differentially expressed between cold and hot tumour groups were detected using ANOVA and filtered by false discovery rate (FDR) q value < 0.01 and fold change > 2.0. Canonical pathways significantly enriched in the genes of interest were identified by Ingenuity Pathways Analysis (IPA) (Ingenuity Systems; http://www.ingenuity.com) based on experimental evidence from the Ingenuity Knowledge Base (release date 23 March 2014). The somatic variants were converted to VCF format and annotated using ANNOVAR (release date 23 August 2013)[32]. Each variant was annotated with known genes, exonic functions, predicted amino acid changes and minor allele frequencies derived from the 1000 Genomes Project (phase 1, release v.3, 23 November 2010) and the NHLBI Exome Sequencing Project (ESP6500SI-V2-SSA137) (EVS)[33]. Synonymous single-nucleotide variants (SNVs) were excluded from further analysis. The variants were then summarized at gene level and patient level for comparison of mutation profiles between the cold and hot tumour groups. Interactions between proteins encoded by genes of interest were retrieved from the STRING database based on high-confidence evidence collected from co-expression data, experiments and databases[34]. SNVs located in selected genes were analysed using the Variant Effect Prediction (http://www.ensembl.org/info/docs/tools/vep/index.html) software in combination with the UniProt database (http://www.uniprot.org). Calls of loss-of-function and gain-of-function were based on existing experimental data obtained from the UniProt data base, while harmful or tolerated effects on the protein structure were predicted using the SIFT prediction algorithm imbedded in the Variant Effect Predictions analysis. A continuous numerical score was generated using the six β-catenin target genes (*EFNB3*, *APC2*, *TCF1*, *c-MYC*, *TCF12*, *VEGFA*) reads. The resulting score was used to align patients based on activity of the β-catenin pathway.

Mice, tumour induction and generation of tumour cell lines. The following mouse strains were gifts from collaborators and were used to generate the mouse models used in this study: *Tyr:Cre-ER* (gifted by L. Chin), *LSL-Braf*^{V600E} (provided by M. MacMahon), *Pten*$^{fl/fl}$ (provided by T. Mak), *LSL-CAT-STA* (provided by F. Gounari), *Rosa26*-LSL-SIY and *Rosa26*-LSL-YFP (Jackson Laboratories, strain 006148) reporter[16,35–38]. As an initial cross, the *Tyr:Cre-ER* mice were crossed onto *LSL-Braf*^{V600E} and subsequently crossed with the *loxP-Pten* mouse strain. Those mice were maintained as *Tyr:Cre-ER*$^{+}$, *LSL-Braf*$^{V600E+/-}$, *Pten*$^{fl/fl}$ and will be referred to as *Braf*^{V600E}/*Pten*$^{-/-}$. Additionally *Tyr:Cre-ER*, *LSL-Braf*^{V600E} mice were crossed to the *LSL-CAT-STA* mouse strain with subsequent crossing to the *Pten*$^{fl/fl}$ strain. Those mouse strains were maintained as *Tyr:Cre-ER*$^{+}$, *LSL-Braf*$^{V600E+/-}$, *LSL-CAT-STA*$^{+/+}$ and *Tyr:Cre-ER*$^{+}$, *LSL-Braf*$^{V600E+/-}$, *Pten*$^{fl/fl}$, *LSL-CAT-STA*$^{+/+}$ and will be referred to as *Braf*^{V600E}/*CAT-STA* or *Braf*^{V600E}/*Pten*$^{-/-}$/*CAT-STA*, respectively. Additionally, the *Braf*^{V600E}/*Pten*$^{-/-}$ and *Braf*^{V600E}/*Pten*$^{-/-}$/*CAT-STA* mice were crossed to the *Rosa26-LSL*-SIY mouse and mice were maintained heterozygote for the *Rosa26* locus. Similarly, *Braf*^{V600E}/*Pten*$^{-/-}$ mice were bred onto the *Rosa26-LSL*-YFP reporter strain, which were also maintained with heterozygous breeders for this locus. Genotyping was performed as described previously[16,35–39] (for primer sequences, see Supplementary Table 5). For tumour induction, 6–10-week-old mice were shaved on the back and 5 µl of 4-OH-tamoxifen (Sigma) at a concentration of 10 mg ml^{-1} (dissolved in acetone) were applied. Subsequently, mice were screened weekly for tumour induction and growth with endpoint criteria of 4,000 mm^3. For tumour cell line generation, a single-cell suspension of the tumour tissue was generated as described later and as its entirety used for subcutaneous injections into Rag-knockout mice (RAGN12-F; Taconic). After tumour outgrowth, the tumour tissue was harvested and re-injected into *Rag*-knockout mice, C57BL/6 mice (Taconic), and adapted to cell culture using DMEM (Gibco) with 10% FCS (Atlanta Biologics), 1× NEAA (Gibco) and 1× MOPS (Sigma). In this work we used one cell line derived from each genotype, *Braf*^{V600E}/*Pten*$^{-/-}$ and *Braf*^{V600E}/*Pten*$^{-/-}$/*CAT-STA*. Additionally, TCR-transgenic 2C T cells were maintained as T-cell donors[40], actin–GFP mice were obtain from Jackson (strain identifier 003291), *Batf3*$^{-/-}$ mice were maintained as bone marrow donors and were originally obtained from K. Murphy[18]. All animal procedures were approved by the Institutional Animal Care and Use Committee of the University of Chicago. Human tumour cell lines were obtained from National Cancer Institute and maintained in RPMI medium supplemented with 10% FCS and 1× NEAA.

Tumour growth, tissue harvest and single-cell suspensions. For tumour outgrowth experiments, mice were treated at the lower back with 4-OH-tamoxifen at day 0. After day 21, tumour masses were measured by assessing length, width and height of major tumour mass using a digital calliper. Measuring the height was a critical parameter to assess tumour growth, since width and length were mainly influenced given by the spread of the TAM solution. Tumour volume T_V was calculated: $T_V = T_L \times T_W \times T_H$, where T_L is tumour length, T_H is tumour height and T_W is tumour width, since the tumour shape was rectangular and flat rather than spherical. The maximum tumour size was reached when the tumour mass reached approximately 10% of the body weight. At the indicated experimental endpoint, tumour tissue was harvested, cleared from remaining skin and minced using razor blades. Subsequently, tumour pieces were digested using the human tumour digestion kit (Miltenyi) in combination with the tissue dissociater (Miltenyi). For flow cytometric analysis and cell sorting, living cells were separated using a ficoll (GE) centrifugation step with subsequent washing of the obtained cells. For generation of tumour cell lines, the cell suspension was used directly after digestion and two washing steps.

Immunohistochemistry and fluorescent immunohistology. The immunohistology staining on human samples was performed by the Human Tissue Resource Center of the University of Chicago using biopsies from malignant melanoma patients. Staining was performed using a CD8-specific monoclonal antibody (CD8 clone C8/144B, NeoMarkers), β-catenin (clone CAT-5H1, Life Technologies) in combination with a secondary goat anti-mouse immunoglobulin G (IgG) conjugated to an alkaline phosphatase (Biocare Medical) was applied. Slides were scanned using a CRi Panoramic Scan Whole Slide Scanner. Positivity for β-catenin staining was obtained first and grading was based on the staining intensity. Subsequently, the number of CD8-positive T cells within one needle biopsy (2.5 mm diameter) was counted using ImageJ cell counter and calculated as number of CD8$^+$ T cells per mm^2. Samples with fewer than 50 CD8$^+$ T cells per mm^2 were considered T-cell-infiltrate low whereas counts >50 per mm^2 were considered as T-cell high, similar to as described previously[41]. For mouse fluorescent immunohistology staining, formalin/paraffin-fixed tissues were used to obtain 5 µm sections for subsequent staining. Staining was performed using the following primary antibodies: anti-CD3 (clone SP7, 1:500, Abcam) and anti-Trp1 (clone EPR13063, 1:500, Abcam) in combination with goat anti-rabbit 594 (JacksonImmuno) and Hoechst counterstain. Slides were imaged using a Zeiss Axiovert 200 with a Hammatsu Orca ER firewire digital monochrome camera.

Flow cytometry and cell sorting. For flow cytometric analysis, washed cells were resuspended in staining buffer (PBS with 10% FCS and 0.5 M EDTA (Ambion)). Cells were incubated with live/dead staining dye (Invitrogen, wavelength 450 nm) and Fc Block (clone 93; Biolegend) for 20 min on ice. Subsequently, specific antibodies were added (Supplementary Table 5) and staining was continued for 40 min on ice. After a washing step, cells were either analysed directly or fixed with 4% PFA (BD) solution for 30 min and stored in a 1% PFA solution until analysis. For staining of TCR-transgenic 2C T cells a TCR specific-biotinylated monoclonal antibody (1B2 clone) was obtained from the University of Chicago Monoclonal Core Facility. Subsequent to live/dead staining, TCR-specific monoclonal antibody was added for 15 min on ice at a 1:100 dilution alone with surface antibodies targeting other antigens added in for an additional 25 min thereafter. After a washing step, a 1:500 dilution of Streptavidin APC was added and incubated on ice for 20 min before cells were fixed in 4% PFA and stored in 1% PFA solution. Flow cytometry sample acquisition was performed on a LSR2B (BD), and analysis was performed using FlowJo software (TreeStar). For cell sorting, staining protocols were carried out similarly under sterile conditions. Cell sorting was performed using an ARIAIIIu (BD) and cells were collected in 100% FCS if further used for *in vitro* analysis or in TriZol Reagent (Invitrogen) if used for RNA isolation. Percentage of T cells was calculated as follows ((100/number of total living cells acquired) × number of CD3$^+$ T cells); number per gram tumour was calculated as follows (number of acquired CD3$^+$ T cells/tumour weight).

T-cell stimulation. 2.5×10^4 sorted T cells from spleen and/or tumour were either stimulated on plates coated with 1 μg ml^{-1} anti-CD3 antibody (145-2C11 clone; Biolegend) and 2 mg ml^{-1} anti-CD28 antibody (37.51 clone BD) in T-cell medium (DMEM, 10% FCS, 1× NEAA, 1× MOPS, 500 μM β-mercapthoethanol (Sigma)) or plated on tissue-culture-treated uncoated plates for 8 h. Following incubation, cells were harvested and resuspended in TriZol Reagent (Invitrogen) for subsequent RNA isolation.

RNA isolation and qRT–PCR. RNA isolation using TriZol was performed according to the manufacturer's instruction. In the case of RNA isolation from whole tumour tissue, a piece of tumour was snap frozen in TriZol at the time of tumour harvest. Before RNA isolation the tissue was thawed at room temperature and homogenization was achieved using a tissue homogenizer (GE) with homogenizer tips (USA Scientific). Subsequent RNA isolation was performed according to the manufacturer's instructions. Reverse transcriptase reaction was performed using High Capacity cDNA RTPCR Kit (Life Technologies) according to instructions and 1 μl of the resulting copy DNA was used for qPCR. qPCR reactions were carried out using Sybr Green or TaqMan master mix (Life Technologies) and defined primer sets or primer/probe sets (probes were obtained from Roche), respectively (Supplementary Table 5). Reactions were run on a 7300 RT PCR system machine (Applied Biosystems) and expression level and fold change were calculated as follows: $\Delta CT = CT_{\text{gene of interest}} - CT_{18S}$; expression level $= 2^{-\Delta CT}$; fold change $= 2^{(\Delta CT_{\text{reference sample}} - \Delta CT_{\text{tested sample}})}$ (ref. 42).

Adoptive T-cell transfer. For adoptive transfer experiments, tumour development was induced and transfer of 1×10^6 T cells was performed when tumour reached near endpoint sizes (approximately 3–4 weeks after induction). Transferred T cells were isolated from gender-matched 2C donor mice using the Miltenyi CD8$^+$ enrichment Kit II for untouched CD8$^+$ T-cell isolation. After isolation, cells were stained with 1 μM CFSE solution (eBioscience) for 8 min at 37 °C before intravenous injection. Tumour tissue, tumour-draining lymph nodes and spleen were harvested 5 days after adoptive transfer of T cells and used for flow cytometric analysis. This short timeframe was chosen to avoid the reported leakiness of the SIY transgene that has been associated with partial T-cell activation within the spleen[16]. For tumour tissues, the entirety of each sample was acquired and the total number of CD3$^+$CD8$^+$ T cells and transferred 2C cells was assessed. The percentage 2C cells was calculated as ((100/CD3$^+$/CD8$^+$ T cells) × 2C) and also the number of 2C cells per gram tumour.

Generation of bone marrow chimaeras. To condition host mice to generate bone marrow chimaeras, indicated mouse strains were irradiated twice with a 3 h interval and a first irradiation dose of 500 rad followed by 550 rad. Twenty-four hours after the second irradiation dose, bone marrow from gender-matched donor mice was isolated from femur and tibia of both legs, washed, and erythrocytes were lysed. 3×10^6 bone marrow cells were injected intravenously to reconstitute the mice. Two-to-three months after bone marrow transfer, tumour development was induced as described previously.

Generation and administration of bone-marrow-derived dendritic cells. For administration of bone-marrow-derived dendritic cells, bone marrow from C57BL/6 mice or GFP–actin mice was collected from the femurs and tibias of both legs. After washing and lysis of erythrocytes, bone marrow cells were cultured in RPMI (Gibco) complete medium (10% FCS, 1× NEAA, 500 μM β-ME) supplemented with 300 ng ml^{-1} Flt3 ligand (eBioscience) for 7 days at a concentration of 2.5×10^6 cells ml^{-1}. Dendritic cells were then activated for 24 h with poly(I:C) (InvivoGen) at a final concentration of 5 μg ml^{-1} (pre-heated for 5 min at 95 °C). Activated Flt3 ligand dendritic cells were frozen in aliquots of 5×10^6 cells in 90% FCS with 10% dimethylsulfoxide (DMSO; Sigma) until use for *in vivo* administration. For each dendritic cell preparation, activation marker expression was analysed using flow cytometry with the majority of cells being CD11c$^+$, CD11b$^+$, predominantly CD8α$^+$ and after activation high expression of CD80, CD86, MHCII and CD40 was observed. Injection of dendritic cells was initiated when the first signs of tumour lesions were identified on mice (2–3 weeks after induction) and were given intra-dermally/intra-tumourally using a 27G (Braintree) needle twice per week at a dose of 1×10^6 dendritic cells per injection.

Gene array analysis of mouse tumour tissue. For gene array analysis, RNA from whole tumour tissue was isolated. Subsequent experimental procedures were performed by the University of Chicago Genomics Core facility using the Illumina MouseWG-6 gene array chip (Illumina) according to the manufacturer's instructions. Subsequent gene lists were analysed from differentially expressed genes with a cut off for at least twofold change between the two analysed cohorts. Significance was determined using a two-way ANOVA test.

Trans-well migration assay. Dendritic cell populations were isolated from lymph nodes and skin of naive 6-week-old C57BL/6 mice. For this purpose, skin tissue was digested in a similar way as tumour tissue and cells from skin and lymph node were stained using the previously described protocol for cell sorting. Subsequently, living, CD45$^+$, CD11c$^+$, CD8α$^-$ or CD8α$^+$ cells were isolated from the lymph node sample as well as living, CD45$^+$, CD11c$^+$ or CD103$^+$ cells from skin samples. Migration assays were performed as described previously with minor adaptations using 5×10^5 cells per well and pre-treatment of dendritic cells with pertussis toxin (Sigma) at a final concentration of 20 ng ml^{-1} for 1.5 h as indicated[43]. As a migration stimulus, CCL4 (R&D) was added to RPMI complete medium at 500 ng ml^{-1} or 48 h conditioned media from *Braf*^{V600E}/*Pten*$^{-/-}$ or *Braf*^{V600E}/*Pten*$^{-/-}$/*CAT-STA* cell lines were used. At the endpoint, cells from the lower compartment as well as the trans-well were harvested and counted using a standard Neubauer counting chamber. Percentage of migrated cells was calculated as follows: count lower well/(count upper well + count lower well) × 100; with the sum of trans-well and lower well being >90% of the input cell count.

ELISA. ELISA assays against murine and human CCL4 were performed using CCL4-specific ELISA kits (R&D) according to the manufacturer's instructions.

siRNA knockdown. Target gene-specific and control siRNAs were obtained from Ambion and can be found in Supplementary Table 5. For knockdown, 3×10^4 tumour cells are plated in 96-well plates at a concentration of 3×10^5 per ml. Opti-MEM (Gibco) was mixed with 1.2 pmol siRNA and 1.5% RNAiMAX reagent (Invitrogen) and added to the culture at a ratio of 1:5. Cells were incubated for 48 h before supernatant was harvested for ELISA assays and cells were collected for RNA or protein extraction.

Western blotting. Cell lysates were generated using RIPA buffer in combination with protein inhibitor (Invitrogen) and protein concentration was determined using Bradford protein assay (Biorad). Denaturated lysates were applied to a 10% SDS–PAGE and blotted using standard procedures. For protein detection, blots were incubated with primary antibodies (β-catenin clone D10A8; β-actin clone 13E5; Cell Signaling) overnight and with secondary antibodies (donkey anti-rabbit-HRP; GE Healthcare) for 2 h. Chemiluminescence was used to visualize the protein bands (GE Healthcare).

ChIP assay. For ChIP assays, the two cell lines, BP and BPC, were grown to 80% confluence in a 10 cm Petri dish. Cells were fixed with 1% formaldehyde solution for 30 min at 37 °C. Subsequent steps were performed using the EpiTect ChIP kit (Qiagen) according to the manufacturer's instructions with some minor adaptations. In brief, the formaldehyde was removed and cells were washed before harvesting using RIPA buffer. Sonication was performed using a water bath sonicator (GE) with the following cycle of 30 s on/15 s off at maximum voltage for 15 min, and this cycle was repeated three times at 4 °C. Chromatin-containing supernatants were incubated with an ATF3-specific antibody (mouse: polyclonal rabbit IgG; human: clone 44C3a, mouse IgG; Abcam) or rabbit/mouse IgG1 isotype (Cell Signaling) for 3 h or overnight at a 1:50 dilution. Pulled-down DNA was used as template for qPCR using Sybr Green master mix and primers (Supplementary Table 5). Results were calculated as followed: $\Delta CT = \Delta CT_{IP} - (\Delta CT_{IP} - \log_2{}^{100})$, fold enrichment $= 2^{(\Delta CT_{iso} - \Delta CT_{IP})}$.

Monoclonal antibody therapy. Therapy using monoclonal antibodies was initiated either when the tumour was first palpable or 7 days after dendritic cell injection was initiated. Mice were assigned to groups in a randomized fashion based on their ear tag number. Antibodies (CTLA-4 clone 9H10, PD-L1 clone 10F.9G2; BioXcell) were administered every other day throughout the experiment at a dose of 100 μg per mouse per treatment and treatment was initiated 3 weeks after tamoxifen application[26].

Statistical analysis. All statistical analyses were performed using GraphPad Prism (GraphPad) with the exception of analyses of the TCGA data set. Unless otherwise noted, all data are shown as mean ± s.e.m. combined with a two-tailed Mann–Whitney *U* test. Significance was assumed with $P \leq 0.05$. For correlation studies, a Gaussian fit was performed to assure normal distribution. All experiments shown were repeated at least in two independent experiments.

30. Li, B. & Dewey, C. N. RSEM: accurate transcript quantification from RNA-Seq data with or without a reference genome. *BMC Bioinformatics* **12,** 323 (2011).
31. Wilkerson, M. D. & Hayes, D. N. ConsensusClusterPlus: a class discovery tool with confidence assessments and item tracking. *Bioinformatics* **26,** 1572–1573 (2010).
32. Wang, K., Li, M. & Hakonarson, H. ANNOVAR: functional annotation of genetic variants from high-throughput sequencing data. *Nucleic Acids Res.* **38,** e164 (2010).
33. The 1000 Genomes Project Consortium. An integrated map of genetic variation from 1,092 human genomes. *Nature* **491,** 56–65 (2012).
34. Jensen, L. J. *et al.* STRING 8—a global view on proteins and their functional interactions in 630 organisms. *Nucleic Acids Res.* **37,** D412–D416 (2009).
35. Suzuki, A. *et al.* High cancer susceptibility and embryonic lethality associated with mutation of the PTEN tumor suppressor gene in mice. *Curr. Biol.* **8,** 1169–1178 (1998).

36. Gounari, F. *et al.* Stabilization of β-catenin induces lesions reminiscent of prostatic intraepithelial neoplasia, but terminal squamous transdifferentiation of other secretory epithelia. *Oncogene* **21,** 4099–4107 (2002).
37. Dankort, D. *et al.* A new mouse model to explore the initiation, progression, and therapy of $BRAF^{V600E}$-induced lung tumors. *Genes Dev.* **21,** 379–384 (2007).
38. Bosenberg, M. *et al.* Characterization of melanocyte-specific inducible Cre recombinase transgenic mice. *Genesis* **44,** 262–267 (2006).
39. Jeong, J., Mao, J., Tenzen, T., Kottmann, A. H. & McMahon, A. P. Hedgehog signaling in the neural crest cells regulates the patterning and growth of facial primordia. *Genes Dev.* **18,** 937–951 (2004).
40. Manning, T. C. *et al.* Antigen recognition and allogeneic tumor rejection in $CD8^+$ TCR transgenic/$RAG^{-/-}$ mice. *J. Immunol.* **159,** 4665–4675 (1997).
41. Erdag, G. *et al.* Immunotype and immunohistologic characteristics of tumor-infiltrating immune cells are associated with clinical outcome in metastatic melanoma. *Cancer Res.* **72,** 1070–1080 (2012).
42. Schmittgen, T. D. & Livak, K. J. Analyzing real-time PCR data by the comparative C_T method. *Nature Protocols* **3,** 1101–1108 (2008).
43. Spranger, S. *et al.* Generation of Th1-polarizing dendritic cells using the TLR7/8 agonist CL075. *J. Immunol.* **185,** 738–747 (2010).

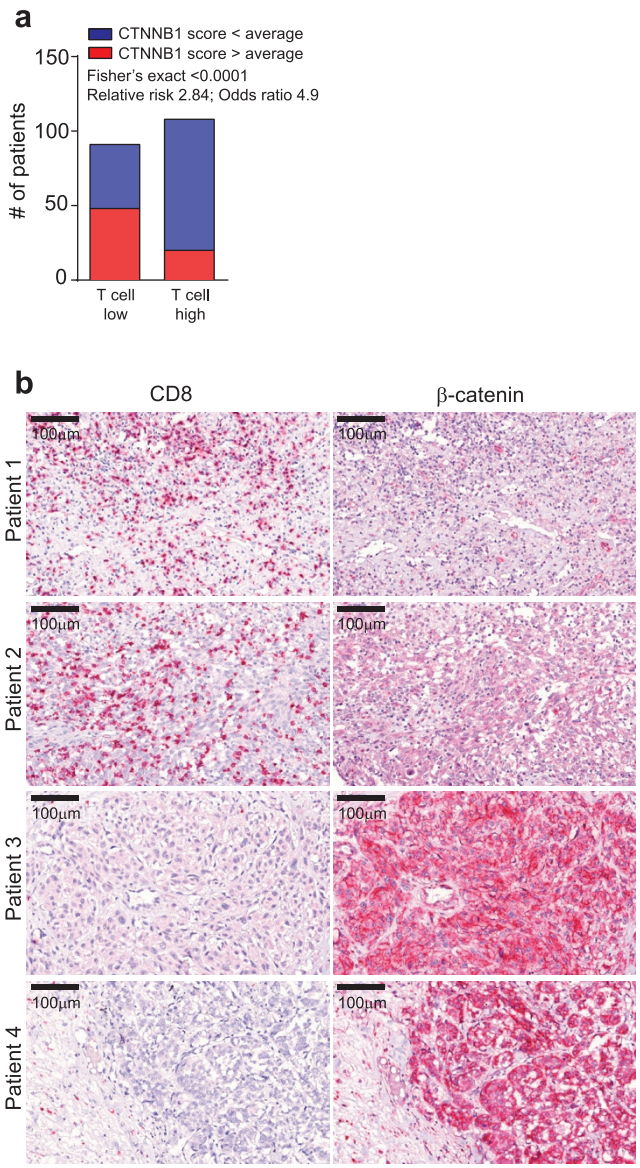

Extended Data Figure 1 | Correlation between active β-catenin and CD8 T-cell infiltrate in human patients. **a**, A continuous numerical score was generated using six β-catenin target genes (*CTNNB1* score). Using this score, patients from the TCGA data set were grouped in high or low *CTNNB1* score (centred on the average score) (low, 91 patients; high, 108 patients). Subsequent correlation analysis was performed using a Fisher's exact test. **b**, Representative examples for CD8 and β-catenin staining in human needle biopsies used for analysis shown in Fig. 1d.

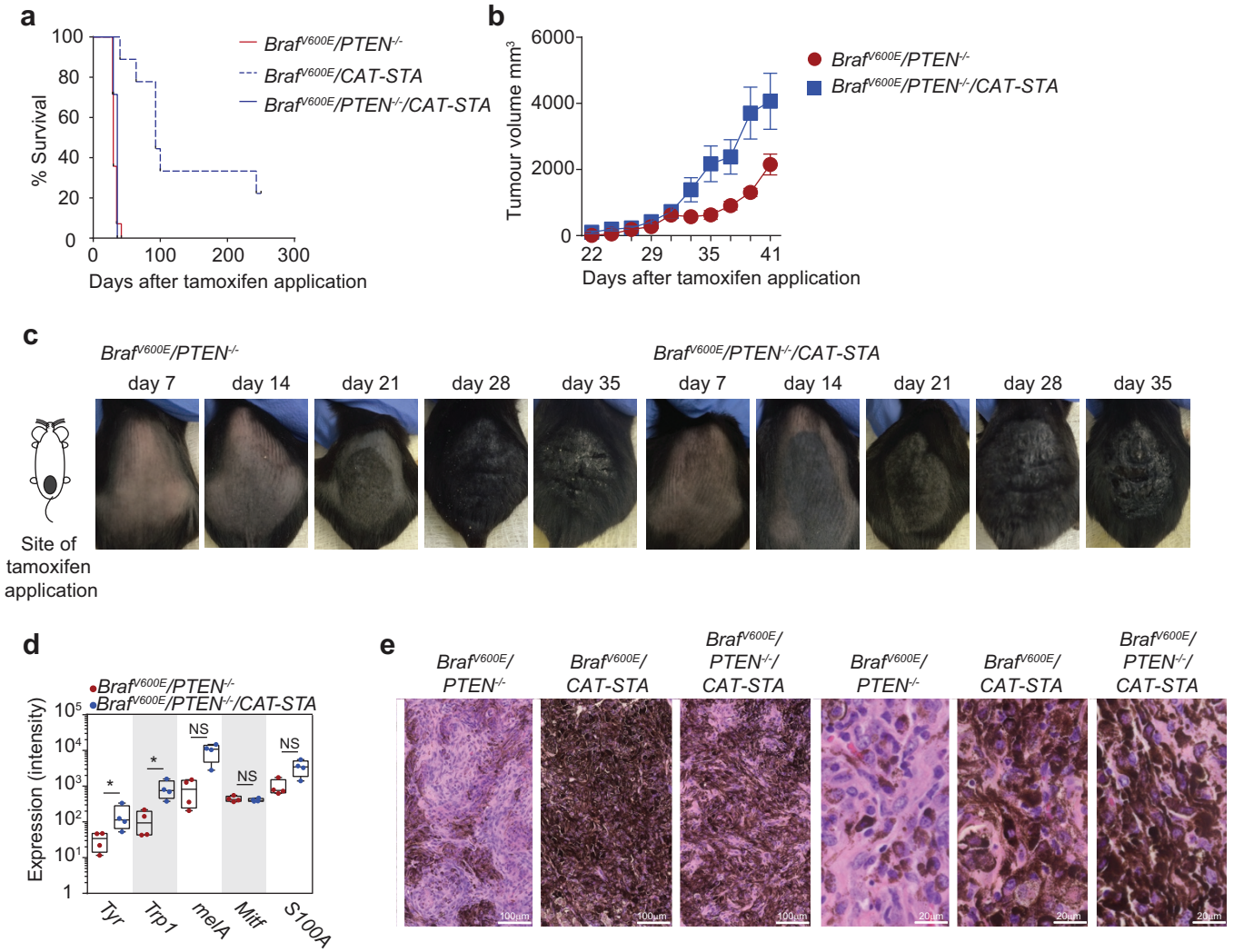

Extended Data Figure 2 | Tumour growth of genetically engineered mice. **a**, Overall survival of all three models: *Braf*^{V600E}/*Pten*$^{-/-}$ with 100% lethality and mean time to death of 31 days ($n = 14$), *Braf*^{V600E}/*CAT-STA* with 85% lethality and mean time to tumour event of 93 days ($n = 8$), and *Braf*^{V600E}/*Pten*$^{-/-}$/*CAT-STA* with 100% lethality and mean time to tumour event of 36 days ($n = 14$). **b**, Tumour outgrowth of *Braf*^{V600E}/*Pten*$^{-/-}$ (red) and *Braf*^{V600E}/*Pten*$^{-/-}$/*CAT-STA* (blue) tumours shown as mm^3 at days after tamoxifen application ($n = 10$). **c**, Representative macroscopic pictures for tumour growth over time when tamoxifen was applied on the lower back of the mouse (see illustration). **d**, Gene array analysis of tumours isolated from GEMs ($n = 4$, Mann–Whitney *U* test). **e**, Histology slides showing representative examples for haematoxylin and eosin stain in all three mouse models (left, ×20, scale bars indicate 100 µm; right, ×100, scale bars indicate 20 µm). *$P \leq 0.05$; NS, not significant.

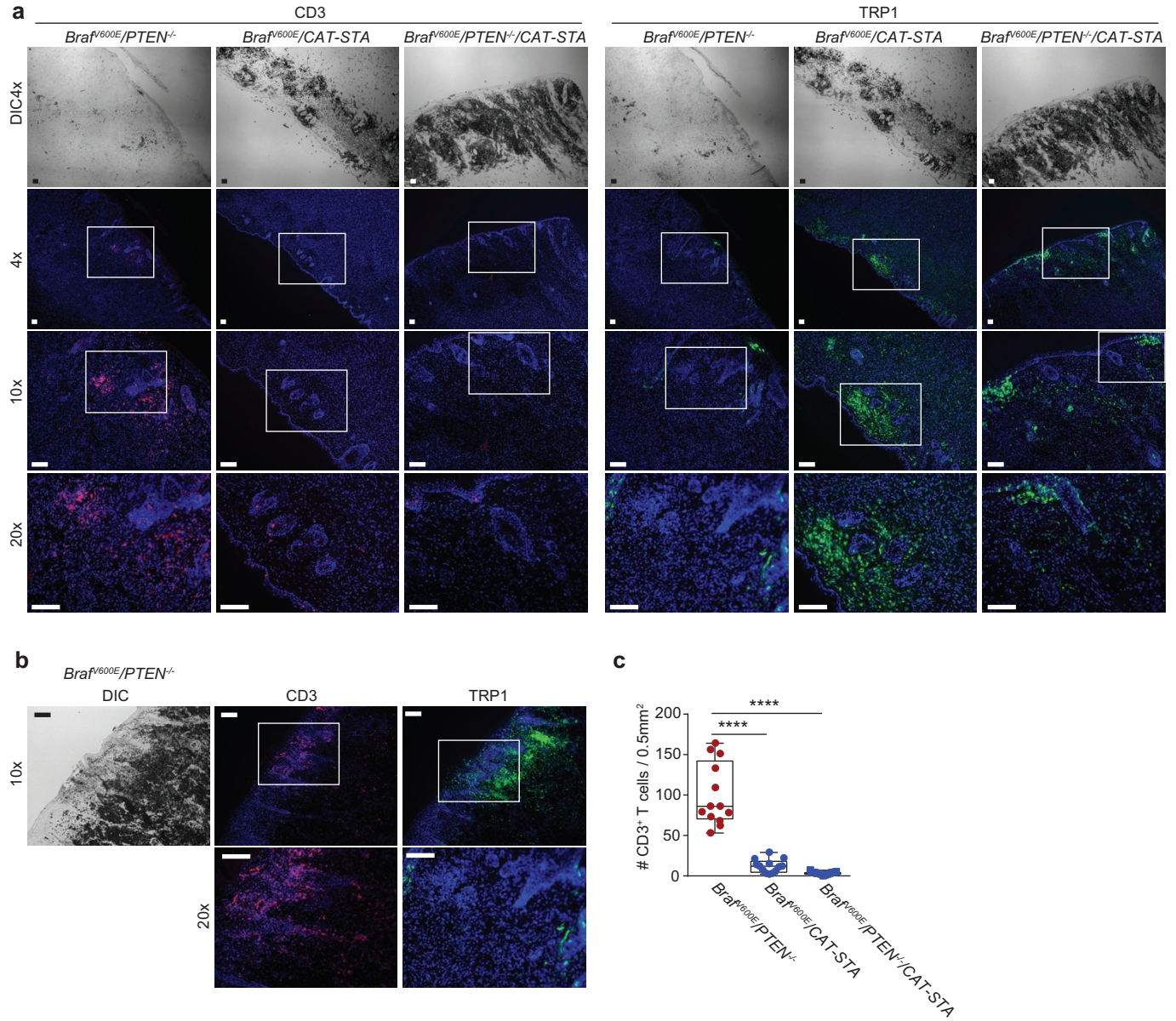

Extended Data Figure 3 | T-cell infiltration of genetically engineered mice. **a**, Representative images of immmunofluorescent staining against CD3 (red, left panel) and TRP1 (green, right panel) in all three tumour tissues (scale bar, 100 μm; ×4, ×10, ×20 with ×4 differential interference contrast (DIC) on top; nuclei Hoechst ×20 CD3 stain as shown in Fig. 1). **b**, Representative immmunofluorescent staining against CD3 (red, left panel) and TRP1 (green, right panel) in a highly pigmented area of $Braf^{V600E}/Pten^{-/-}$ tumour tissues (scale bar, 100 μm; ×10, ×20 with ×10 DIC left) excluding that the lack of T cells is associated with increased pigmentation (nuclei Hoechst). **c**, Numbers of $CD3^+$ T cells were counted within 13 different fields (0.5 mm × 1 mm) from two tumour samples. Mean of 12 T cells or 3.2 T cells per 0.5 mm^2 in $Braf^{V600E}/CAT\text{-}STA$ or $Braf^{V600E}/Pten^{-/-}/CAT\text{-}STA$ tumours, respectively, versus 100 T cells per 0.5 mm^2 in $Braf^{V600E}/Pten^{-/-}$ tumours. Data are given as mean with minimum and maximum, as well as individual values. Statistical analysis was performed using Mann–Whitney *U* test. $^{****}P \leq 0.0001$.

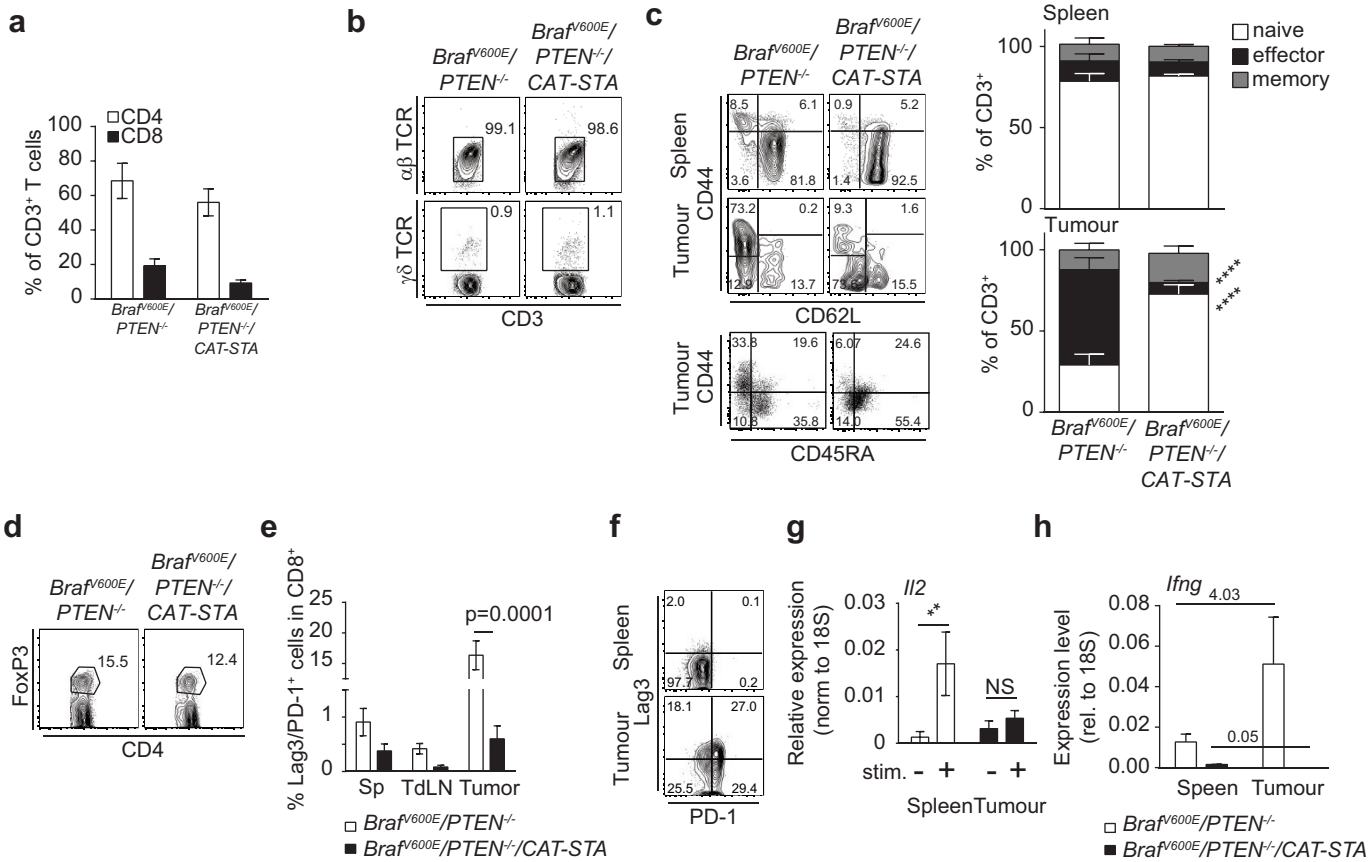

Extended Data Figure 4 | Characterization of the T-cell infiltrate in *Braf^{V600E}/Pten$^{-/-}$/CAT-STA* mice. **a**, Distribution of T-cell subsets in *Braf^{V600E}/Pten$^{-/-}$* and *Braf^{V600E}/Pten$^{-/-}$/CAT-STA* tumours ($n = 6$). **b**, **c**, Representative flow cytometry plots to discriminate αβ-TCR T cells and γδ-TCR T cells (**b**), naive ($CD62L^+CD44^-$) and effector ($CD62L^-CD44^+$) T cells (pre-gated on $CD3^+CD8^+$ T cells), and one representative example of CD44/CD45RA staining (**c**). Quantification of naive ($CD62L^+CD44^-CD45RA^+$), effector ($CD62L^-CD44^+CD45RA^-$) and memory ($CD62L^+CD44^+CD45RA^-$) T cells is indicated on the right ($n = 6$). **d**, Representative flow cytometry plots of $FoxP3^+$ T regulatory cells ($n = 6$). **e**, Quantification and comparison of PD-1/Lag3 double-positive T cells in *Braf^{V600E}/Pten$^{-/-}$* and *Braf^{V600E}/Pten$^{-/-}$/CAT-STA* tumours ($n = 12$). **f**, Representative flow cytometry of PD-1- and Lag3-positive T cells (pre-gated on $CD3^+CD8^+$ T cells) in *Braf^{V600E}/Pten$^{-/-}$* tumours. **g**, *Il2* transcripts present in sorted $CD3^+$ T cells from *Braf^{V600E}/Pten$^{-/-}$* tumours and spleen ($n = 10$). **h**, *Ifng* transcripts present in sorted $CD3^+$ T cells from *Braf^{V600E}/Pten$^{-/-}$* and *Braf^{V600E}/Pten$^{-/-}$/CAT-STA* mice ($n = 10$). **i**, Expression level of PD-L1 in whole tumour tissue from both mouse models assessed by qRT–PCR ($n = 8$). **j**, Flow cytometric analysis of PD-L1 expression of non-haematopoietic tumour cells ($CD45^-$), $CD45^+CD11c^+$ dendritic cells (DC) and $CD45^+CD3^+$ T cells. Shown is a representative example as histogram (grey isotype, red *Braf^{V600E}/Pten$^{-/-}$*; blue, *Braf^{V600E}/Pten$^{-/-}$/CAT-STA*) with mean fluorescent intensity of $n = 3$ given each histogram (red, *Braf^{V600E}/Pten$^{-/-}$*; blue, *Braf^{V600E}/Pten$^{-/-}$/CAT-STA*). **k**, Percentage of $Gr1^+$ cells within the $CD11b^+$ fraction of the tumour immune cell infiltrate ($n = 8$; absolute numbers *Braf^{V600E}/Pten$^{-/-}$*: 1,047 ± 418 cells per gram tumour to *Braf^{V600E}/Pten$^{-/-}$/CAT-STA*: 739 ± 185 cells per gram tumour; $P = 0.7429$). All data are mean ± s.e.m., Mann–Whitney *U* test.*$P \leq 0.05$, **$P \leq 0.01$, ****$P \leq 0.0001$; NS, not significant.

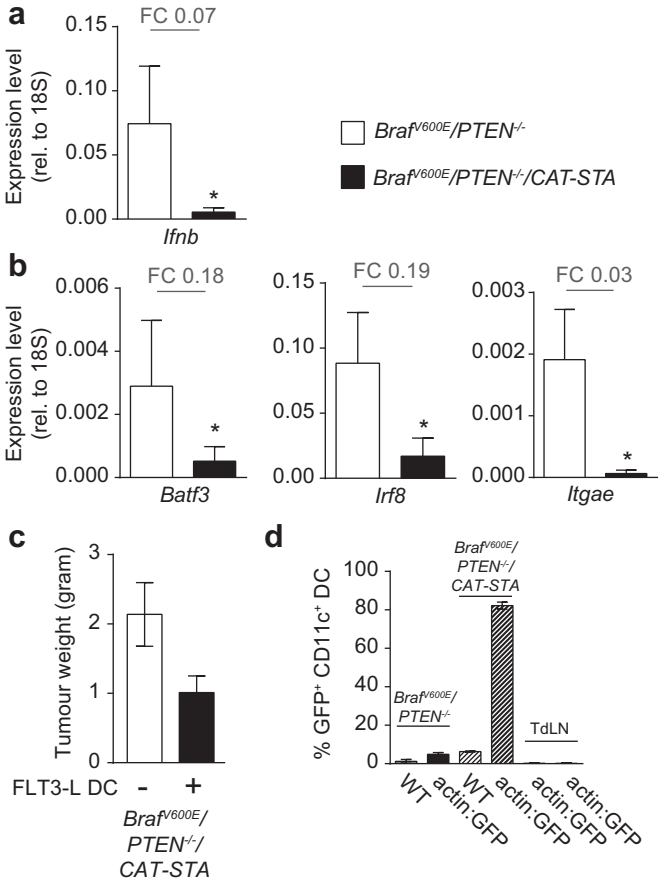

Extended Data Figure 5 | Injection of Flt3 ligand-derived dendritic cells into tumours of *Braf*^{V600E}/*Pten*$^{-/-}$/*CAT-STA* mice is sufficient to overcome the lack of CD103^{+} dermal dendritic cells. **a**, Expression level of *Ifnb* in CD45^{+}CD11c^{+} sorted dendritic cells from tumours from *Braf*^{V600E}/*Pten*$^{-/-}$ (open bars) and *Braf*^{V600E}/*Pten*$^{-/-}$/*CAT-STA* (filled bars) mice. FC, fold change. **b**, Expression level of *Batf3*, *Irf8* and *Itgae* in sorted dendritic cells. Fold change is indicated in each graph ($n = 8$). **c**, Mean ($\pm$ s.e.m.) tumour weight of *Braf*^{V600E}/*Pten*$^{-/-}$/*CAT-STA* assessed at the endpoint of the experiment depicted in Fig. 3e, after intra-tumoural injection of dendritic cells. **d**, Per cent of GFP^{+}CD11c^{+} dendritic cells (DC) present at the tumour site after injections of Flt3 ligand-derived dendritic cells from actin–GFP mice. Depicted are the percentages detected in the tumour of both genotypes injected with either wild-type or actin–GFP dendritic cells as well as in the TdLNs for the actin–GFP injected mice ($n = 4$). All data are mean $\pm$ s.e.m., Mann–Whitney *U* test. *$P \leq 0.05$.

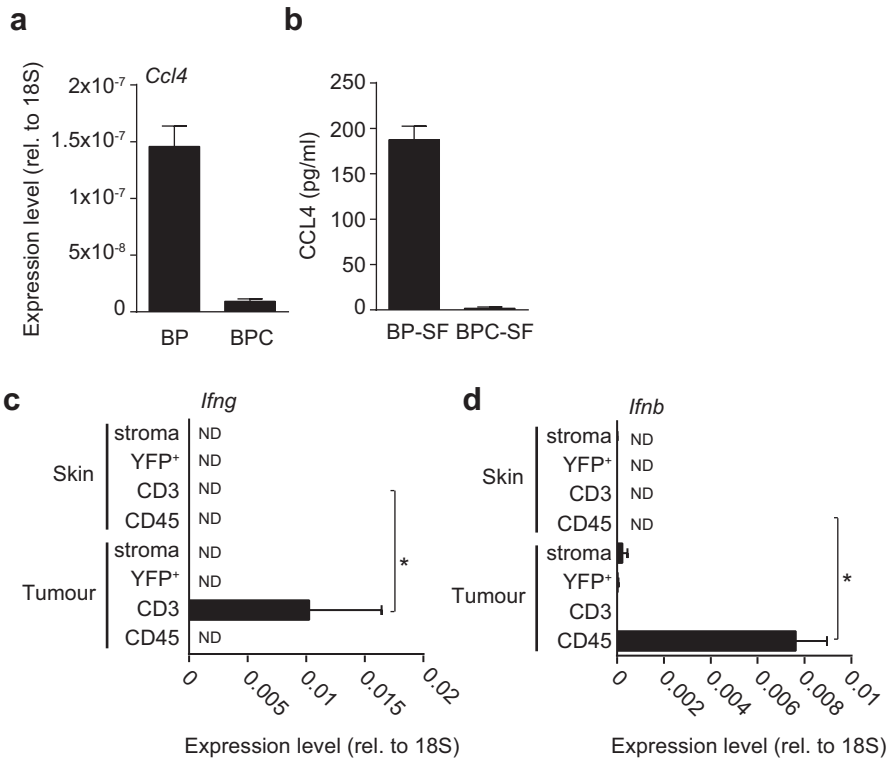

Extended Data Figure 6 | Chemokine expression patterns indicate that CCL4 expression from tumour cells is directly inhibited by active β-catenin-signalling. **a**, Expression of *Ccl4* mRNA in established tumour cell lines BP and BPC (8 independent experiments). **b**, Amount of secreted CCL4 in 48 h conditioned BP and BPC tumour cell supernatants, assessed by ELISA (4 independent experiments). **c**, **d**, Control qRT–PCR for the experiment shown in Fig. 4e with *Ifnb* expression (c) and *Ifng* expression (d) ($n = 6$). ND, not detected. All data are mean ± s.e.m., Mann–Whitney *U* test. $^*P \leq 0.05$.

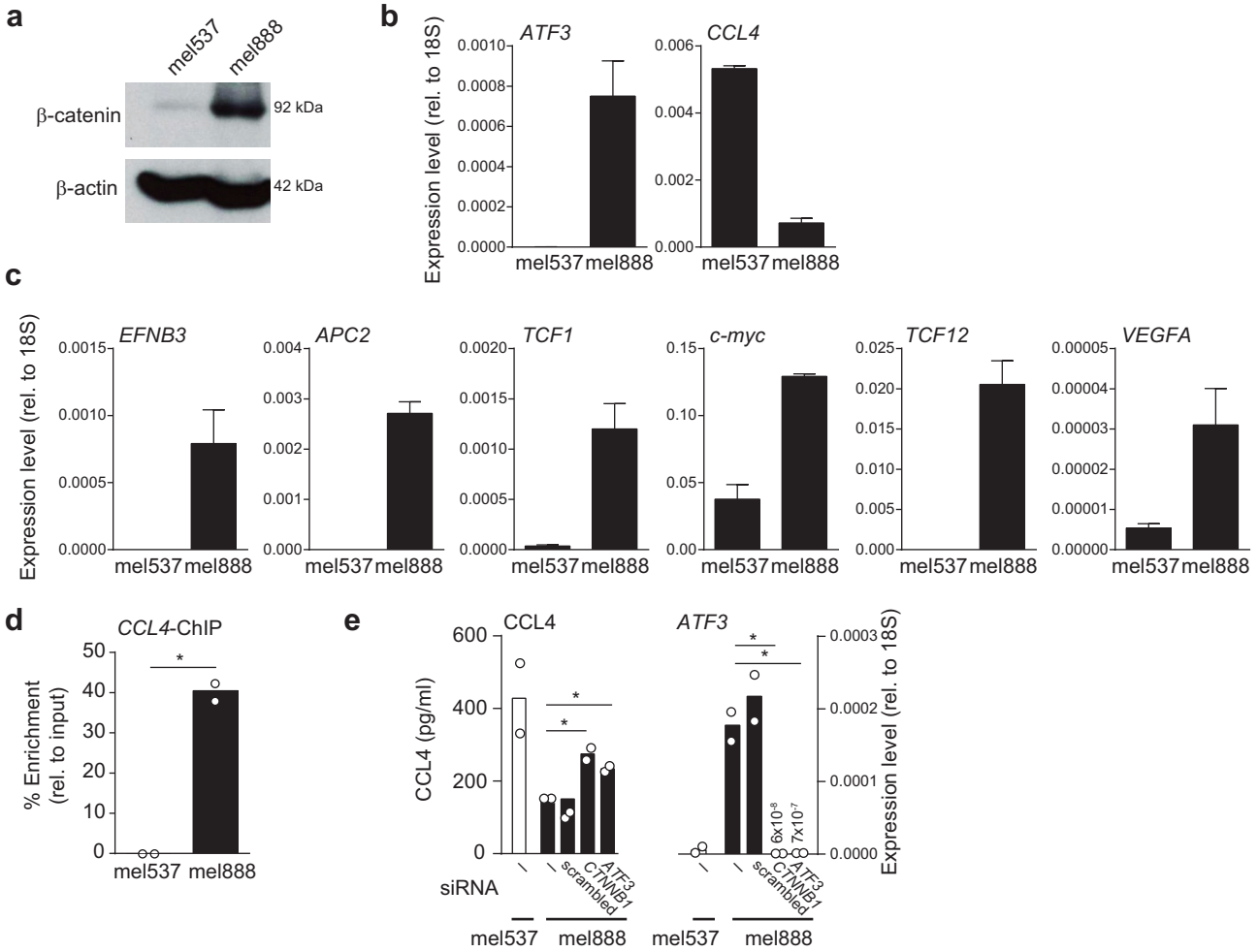

Extended Data Figure 7 | Active β-catenin signalling blocks CCL4 production in human melanoma cell lines. **a**, Western blot on mel537 and mel888 showing stabilized β-catenin expression. **b**, Expression level of human *ATF3* and human *CCL4* in mel537 and mel888 (three independent experiments, duplicates per experiment). **c**, Expression level of β-catenin target genes in mel537 and mel888. **d**, ATF3-specific ChIP assay in mel537 and mel888 cell lines for the *CCL4* gene locus (two independent experiments, duplicates per experiment). **e**, CCL4 secretion (left) and *ATF3* transcription levels (right) after siRNA-mediated knockdown of *CTNNB1 and ATF3* in mel537 and mel888 assessed by ELISA or qRT–PCR, respectively (two independent experiments, duplicates per experiment). All data are mean ± s.e.m., Mann–Whitney *U* test. $^*P \leq 0.05$.

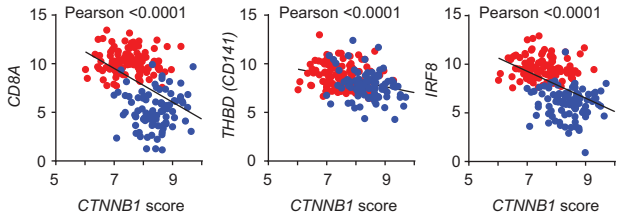

Extended Data Figure 8 | β-Catenin target gene expression correlates inversely with markers for human BATF3-lineage dendritic cells and T cells. Pearson correlation of *CTNNB1* score with *CD8A* ($R^2 = 0.214$), *THBD* ($R^2 = 0.109$) and *IRF8* ($R^2 = 0.2374$) (red indicates T-cell-signature high, blue indicates T-cell-signature low).

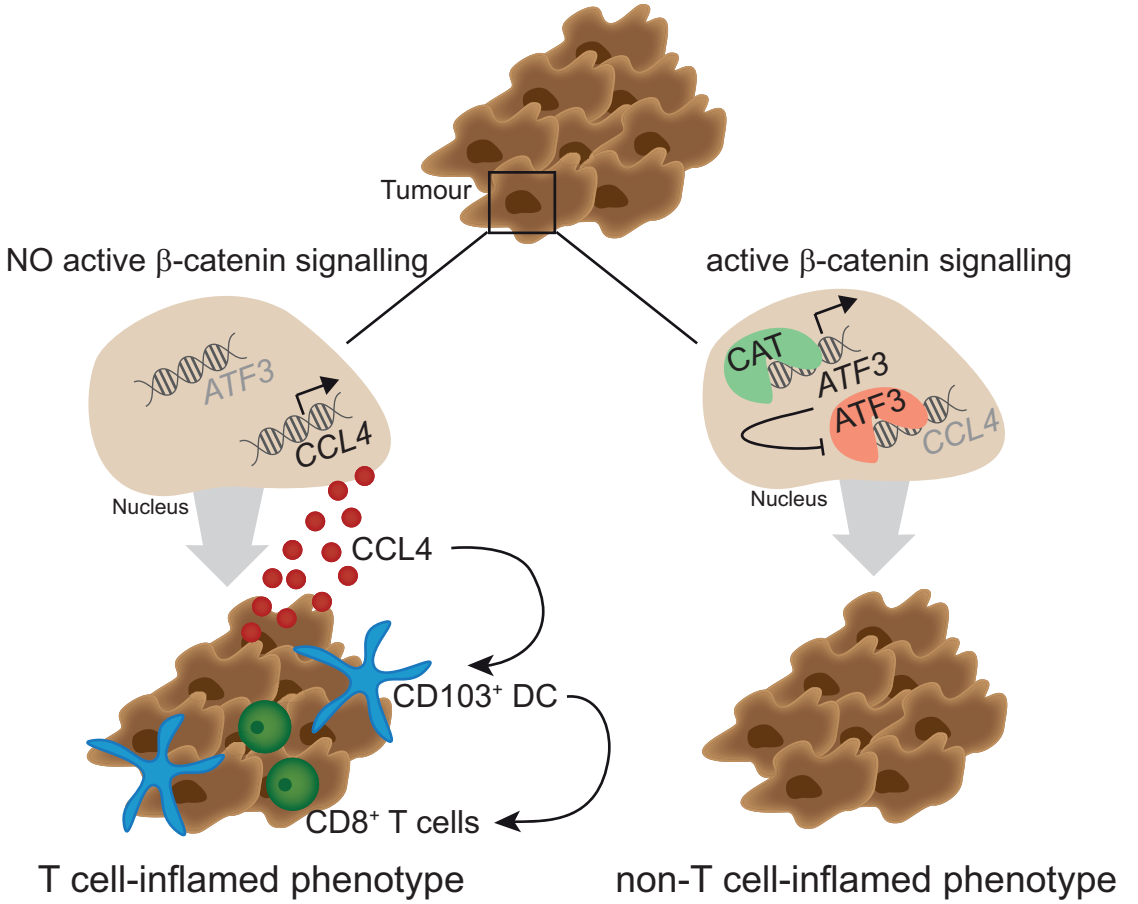

Extended Data Figure 9 | Graphical summary. Left, tumour without active β-catenin signalling in which *ATF3* transcription is not induced and thus *CCL4* (red circles) is transcribed and secreted. Downstream $CD103^+$ dendritic cells (DC) (blue) are attracted and subsequent activation of $CD8^+$ T cells (green) is enabled. Right, tumour with active β-catenin signalling (green), which leads to induction of *ATF3* transcription (red), which in turn leads, among others effects, to suppression of *CCL4* transcription. This leads to an active escape from the anti-tumour immune response since dendritic cell recruitment is insufficient.